Critical and Spin-Wave Scattering of Neutrons from Iron*

M. F. COLLINS,† V. J. MINKIEWICZ, R. NATHANS, L. PASSELL, AND G. SHIRANE
Physics Department, Brookhaven National Laboratory, Upton, New York 11973
(Received 26 September 1968)

The wavelength and frequency dependence of neutrons magnetically scattered from iron has been studied with high resolution from low temperatures to $1.05T_c$. At low temperatures, the spin waves can be satisfactorily described in terms of a model Hamiltonian containing Heisenberg and dipole-dipole terms. The spin-wave energies vary as $1-T/T_c$ to the power 0.37 ± 0.03 over a temperature range $0.005<1-T/T_c<0.2$. At a temperature a few degrees below T_c, the spin waves become over-critically damped. In the spin-wave region, no peak corresponding to a diffusive mode has been observed in the scattering, in contrast to the antiferromagnet $RbMnF_3$, where the existence of such a peak has been clearly demonstrated. Above T_c, in the hydrodynamic region, the scattering can be described in terms of a diffusion equation. The diffusion constant and static susceptibility vary as $1-T_c/T$ to the powers 0.14 ± 0.04 and 1.30 ± 0.06, respectively, over the temperature range $0.008<1-T_c/T<0.05$. The observed power laws indicate that near the Curie temperature the spin-wave energies vary with temperature in the same way as the magnetization, while the diffusion constant varies more slowly with temperature than has been predicted. In agreement with earlier measurements, the data for the static susceptibility indicate that the power law of the divergence is close to 1.30. Values in the range 1.33–1.43 are predicted by high-temperature expansion techniques. There is evidence for the existence of a strongly damped propagating mode in the transition region at and above T_c. At the critical temperature, linewidths scale as the wave vector to the power 2.7 ± 0.3; within error, this is the same as the power 2.5 predicted on the basis of the dynamic scaling laws.

I. INTRODUCTION

AMONG the ferromagnetic materials studied by the methods of neutron scattering, iron occupies a unique position. In fact, the dynamics of the spins in iron has become one of the classic problems in the field of magnetism. At present, relatively complete studies of the long-wavelength spin waves are available at temperatures well below the Curie temperature T_c,[1,2] and there also exist extensive measurements of the critical scattering above T_c. These latter have given considerable insight into the properties of the diffusive modes.[3–6]

Although experiment has generally been in reasonable accord with theory, there are a few notable points of disagreement. One of the more puzzling of these concerns the spin-diffusion constant which describes the dynamics of the spin fluctuations in the critical region. According to conventional diffusion theory, the diffusion constant should show a temperature dependence of the form $(1-T_c/T)^{1/3}$; surprisingly, in the data currently available there is no indication of any temperature variation.

In searching for an explanation of this apparent contradiction, both Marshall[7] and Halperin and Hohenberg[8] have suggested that highly damped propagating modes may exist in iron even at temperatures slightly above T_c. They argue that at these temperatures either diffusive modes, propagating modes, or both can contribute to the scattering. The type of excitation will depend on whether the scattering vector q is large or small compared to κ_1, where $1/\kappa_1$ represents the spin-correlation range.

By definition, the hydrodynamic region is the region $q<\kappa_1$ in which only diffusive modes are involved in the scattering. Near T_c this region will be very restricted because κ_1 is very small. Therefore, for the values of q generally used in neutron experiments, we can only expect diffusive modes to be uniquely excited at temperatures well above T_c, while near T_c both damped propagating modes and diffusive modes will be encountered. Thus, it is likely that the existing measurements fail to show the expected temperature variation of the spin-diffusion constant because they were not made entirely in the hydrodynamic region.

With these ideas in mind, we recently undertook a comprehensive program of inelastic scattering measurements on iron. As will be evident, the intense slow-neutron flux at the Brookhaven High-Flux Beam Reactor has allowed us to improve materially on earlier work. While previous measurements relied either on scattering surface techniques or depended for their interpretation on the assumption that only diffusive modes were being observed, we have been able to measure the scattering generally. Our measurements extend over a wide range from temperatures well below

* Work performed under the auspices of the U. S. Atomic Energy Commission.

† On leave from Atomic Energy Research Establishment, Harwell, England.

[1] G. Shirane, R. Nathans, O. Steinsvoll, H. A. Alperin, and S. J. Pickart, Phys. Rev. Letters **15**, 146 (1965).

[2] M. W. Stringfellow, J. Phys. **C1**, 950 (1968).

[3] B. Jacrot, J. Konstantinovic, G. Parette, and D. Cribier, *Inelastic Scattering of Neutrons in Solids and Liquids* (International Atomic Energy Agency, Vienna, 1963), p. 317.

[4] L. Passell, K. Blinowski, T. Brun, and P. Nielsen, Phys. Rev. **139**, A1866 (1965).

[5] S. Spooner and B. L. Averbach, Phys. Rev. **142**, 291 (1966).

[6] D. Bally, B. Grabcev, A. M. Lungu, P. Papovici, and M. Totia, J. Phys. Chem. Solids **28**, 1947 (1967).

[7] W. Marshall, Natl. Bur. Std. (U. S.) Misc. Publ. 273 (1965).

[8] B. I. Halperin and P. Hohenberg (private communication).

T_c, where spin-wave modes are clearly defined, through the critical region to temperatures above T_c where the diffusive modes are dominant. Particular emphasis has been placed on measurements in the neighborhood of T_c in order to follow the transition from spin waves at the one extreme to diffusive modes at the other.

In the following sections, the experiments will be described in detail. Section II contains a brief review of the theoretical background; this divides naturally into two interrelated parts, a consideration of the magnetic scattering of neutrons and a description of the dynamics of spins in a ferromagnet. Section III discusses the experimental technique, with special emphasis on the treatment of the instrumental resolution function. In Sec. IV, the experimental data are presented and the interpretation is discussed, and in Sec. V we consider the implications of the results as they affect both the theory of spin dynamics and the future direction of inelastic scattering experiments.

We should also note that some aspects of this work have been mentioned briefly in the literature.[9-11]

II. THEORY

A. Cross Section

The cross section for the inelastic scattering of neutrons by a system of N spins per unit solid angle Ω per unit energy E is

$$\frac{d^2\sigma}{d\Omega dE}=\left(\frac{\gamma e^2}{mc^2}\right)^2\frac{N}{\hbar}\frac{k_1}{k_0}[f(\mathbf{Q})]^2\mathcal{S}(\mathbf{Q},\omega). \quad (1)$$

The first term in brackets has a numerical value of $0.292b$, $f(\mathbf{Q})$ is the atomic form factor, and $\mathbf{Q}$ and ω are defined by

$$\hbar\omega=(\hbar^2/2m)(k_0^2-k_1^2)$$

and

$$\mathbf{Q}=\mathbf{k}_0-\mathbf{k}_1=\boldsymbol{\tau}+\mathbf{q},$$

with $\mathbf{k}_0$ and $\mathbf{k}_1$ the incident and scattered neutron wave vectors, $\boldsymbol{\tau}$ a reciprocal-lattice vector, and m the mass of the neutron. For systems of interest in the present work, $\mathcal{S}(\mathbf{Q},\omega)$ is given by[12,13]

$$\mathcal{S}(\mathbf{Q},\omega)=\frac{\hbar}{\pi g^2\mu^2}\sum_\alpha(1-\hat{Q}_\alpha^2)\left[1-\exp\left(-\frac{\hbar\omega}{kT}\right)\right]^{-1}\times\mathrm{Im}[\chi^\alpha(\mathbf{Q},\omega)]+\mathcal{S}_B(\mathbf{Q},\omega), \quad (2)$$

with $\hat{Q}_\alpha$ the α-direction cosine of $\mathbf{Q}$ and χ the generalized susceptibility of the scattering system. All of the dynamics of the spin system are expressed by the frequency dependence of $\chi(\mathbf{Q},\omega)$. $\mathcal{S}_B(\mathbf{Q},\omega)$ is an elastic Bragg scattering term which is of no interest for the present work and will not be considered further.

It is sometimes convenient to consider the static susceptibility as well as the frequency-dependent susceptibility. This can be derived from the frequency-dependent susceptibility by the relationship

$$\chi^\alpha(\mathbf{Q})=\pi^{-1}\int_{-\infty}^{\infty}\mathrm{Im}[\chi^\alpha(\mathbf{Q},\omega)]\omega^{-1}d\omega.$$

For data taken in the critical region, $kT\gg\hbar\omega$ for all frequencies which contribute significantly to the scattering. The Boltzmann factor in Eq. (2) can then be expanded and it follows that

$$\int_{-\infty}^{\infty}\mathcal{S}(Q,\omega)d\omega=\left(\frac{kT}{g^2\mu^2}\right)\sum_\alpha(1-\hat{Q}_\alpha^2)\chi^\alpha(Q), \quad (3)$$

neglecting the contribution of $\mathcal{S}_B(\mathbf{Q},\omega)$, which is confined solely to $\mathbf{Q}=\boldsymbol{\tau}$. This equation relates $\chi(\mathbf{Q})$ to the experimentally observed $\mathcal{S}(\mathbf{Q},\omega)$.

It is also possible to formulate the scattering in terms of spin-correlation functions. Van Hove[14] showed that such a procedure gives

$$\mathcal{S}(\mathbf{Q},\omega)=(2\pi)^{-1}\sum_\alpha(1-\hat{Q}_\alpha^2)\times\sum_{\mathbf{R}}\int_{-\infty}^{\infty}\exp(i\mathbf{Q}\cdot\mathbf{R}-i\omega t)dt\langle S_0^\alpha(0)S_{\mathbf{R}}^\alpha(t)\rangle, \quad (4)$$

where $S_{\mathbf{R}}^\alpha(t)$ is the α component of spin on the atom at $\mathbf{R}$ at time t.

B. Spin Dynamics and Critical Fluctuations

Above the critical temperature T_c, the susceptibility χ^α becomes independent of α for materials of cubic symmetry. Below T_c we can define a direction of magnetization z so that the susceptibility has two components, χ^z and $\chi^x=\chi^y$. All of our measurements were made in zero magnetic field (less than 5 Oe) so that for randomly oriented domains we observed the average value of $\chi^z+\chi^x+\chi^y$.

The present data are confined to the long-wavelength components of the susceptibility where critical fluctuations are expected to give large effects near T_c. This allows us to use the quantity qR, where R is an interaction distance, as an expansion parameter in some of the theoretical expressions to be quoted.

It is customary to define an inverse correlation range parameter κ_1 for the critical fluctuations. Both Marshall and Halperin and Hohenberg use this parameter as a basis for defining three distinct regions for critical phenomena as shown in Fig. 1. The first region is for $q<\kappa_1$ and $T<T_c$ and will be called the *spin-wave region*;

[9] G. Shirane, V. J. Minkiewicz, and R. Nathans, J. Appl. Phys. **39**, 383 (1968).
[10] M. F. Collins, R. Nathans, L. Passell, and G. Shirane, Bull. Am. Phys. Soc. **13**, 616 (1968).
[11] M. F. Collins, R. Nathans, L. Passell, and G. Shirane, Phys. Rev. Letters **21**, 99 (1968).
[12] T. Izuyama, D. Kim, and R. Kubo, J. Phys. Soc. Japan **18**, 1025 (1963).
[13] W. Marshall, Atomic Energy Research Establishment Report No. T.P. 200, 1966 (unpublished); R. D. Lowde and W. Marshall, Rept. Progr. Phys. (to be published).
[14] L. Van Hove, Phys. Rev. **95**, 1374 (1954).

the second region for $q>\kappa_1$ gives a *transition region*; and finally for $q<\kappa_1$ and $T>T_c$ there is the *hydrodynamic region*. One of the major objectives of this experiment was to examine the scattering to determine whether well-defined regions could actually be identified experimentally.

Let us summarize for later reference some of the relevant features of spin dynamics in each of the three regions.

1. Spin-Wave Region

Assuming a Heisenberg Hamiltonian and $T\ll T_c$, transverse susceptibilities χ^x and χ^y are associated with spin waves which have at long wavelengths energies E_H given by the expression[15]

$$E_H=Dq^2+Eq^4+i\eta q^4, \tag{5}$$

where D, E, and η are all real. There are no fluctuations in the z component of spin.

For real ferromagnets, there is also a dipole-dipole force between spins. When this is included in the Hamiltonian, the spin-wave energy becomes[16]

$$E_S=(E_H^2+4\pi M_0 \sin^2\theta_q\, g\mu E_H)^{1/2} \tag{6}$$

for zero applied field. θ_q is the angle between $\mathbf{q}$ and the z axis and M_0 is the zero-field magnetization. The cross section for neutron scattering from such a spin system has been given by Lowde[17] for the case $\eta=0$. For our purposes, the most important feature of the expression is that for any given value of $\mathbf{q}$ there is a term $\delta(\hbar\omega\pm E_s)$ which implies that scattering occurs only at the two discrete energy transfers E_s and $-E_s$.

As the temperature rises towards T_c the parameters D, E, and M_0 decrease while η increases. Near T_c spin-wave theory does not give reliable values for these parameters and there has been some controversy as to whether or not D in particular goes to zero at $T=T_c$.

Recently Halperin and Hohenberg,[18] applying dynamic scaling-law arguments,[19] have predicted that

$$D\propto(T_c-T)^{1/3} \quad \text{and} \quad \eta\propto(T_c-T)^{-1} \tag{7}$$

near T_c. Thus, according to Halpern and Hohenberg, D should go to zero at $T=T_c$, although the inverse power law for η implies that the spin wave becomes over-critically damped at some temperature less than T_c.

M_0 is also predicted to vary with temperature according to the same $\frac{1}{3}$ power law as D. Thus, it is to be expected that at a given value of q the fractional shift of the spin-wave energy due to the presence of dipole-dipole forces will remain temperature-independent.

[15] B. I. Halperin and P. Hohenberg (private communication).
[16] T. Holstein and H. Primakoff, Phys. Rev. **58**, 1098 (1940).
[17] R. D. Lowde, J. Appl. Phys. **36**, 884 (1965).
[18] B. I. Halperin and P. Hohenberg, Phys. Rev. Letters **19**, 700 (1967); and (private communication).
[19] R. A. Ferrell, N. Menyhard, H. Schmidt, F. Schwabl, and P. Szepfalusy, Phys. Rev. Letters **18**, 891 (1967).

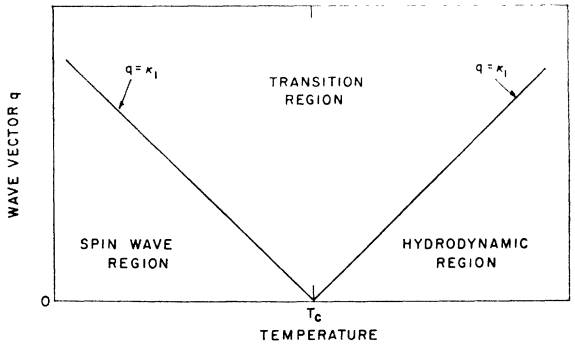

FIG. 1. Schematic diagrams showing the three regions near the critical temperature T_c. The spin-wave region is the region where the temperature is less than T_c and the wave vector q is less than κ_1, the critical range parameter; the transition region is the region where $q>\kappa_1$ and the hydrodynamic region where $q<\kappa_1$ and the temperature is above T_c.

Near T_c there will be an additional contribution to the scattering from fluctuations in the z component of spin. Both diffusive[20–22] and propagating[23,24] terms in χ^z have been suggested in the literature but the actual form of χ^z is still on open question.

2. Transition Region

This is the most difficult of the three regions to treat and theoretical work so far has not passed beyond the "qualitative description" stage. As far as we can determine, Marshall[7] seems to have made the first attempt. He suggested that the scattering should be described in terms of a diffusive mode, as in the hydrodynamic region, and also of another mode which is partially diffusive and partially propagating in character. This second mode has a decreasing influence on the scattering as the temperature is raised and the hydrodynamic region is approached.

An over-all picture on these lines is fairly widely accepted now. Problems arise in trying to make the discussion more quantitative and in particular to answer the question of whether or not any propagating modes are over-crtically damped at and above T_c. Beeby and Hubbard[25] and Bennett,[26] using different approaches, have suggested that such modes may not always be over-critically damped above the Curie temperature. On the other hand, Halperin and Hohenberg,[18] using the dynamic scaling laws, seem to suggest that such modes are over-critically damped. They further make a prediction that the characteristic width Γ of the frequency spectrum $S(\mathbf{q},\omega)$ right at the Curie

[20] R. J. Elliott and W. Marshall, Rev. Mod. Phys. **30**, 75 (1958).
[21] P.-G. de Gennes, Centre à l'Energie Atomique Report No. 925, 1959 (unpublished).
[22] H. Mori and K. Kawasaki, Progr. Theoret. Phys. (Kyoto) **27**, 529 (1962).
[23] Y. V. Galager, Zh. Eksperim. i Teor. Fiz. Pis'ma v Redaktsiyu JETP Letters **2**, 1 (1965).
[24] G. Reiter, Phys. Rev. Letters **20**, 1170 (1968).
[25] J. L. Beeby and J. Hubbard, Phys. Letters **26A**, 376 (1968).
[26] H. S. Bennett (private communication).

temperature should vary with q according to the relationship

$$\Gamma \sim q^{5/2}. \tag{8}$$

3. Hydrodynamic Region

Diffusive modes are expected to dominate the scattering when q is less than κ_1 and $T > T_c$. For these modes, a close analogy exists between the critical scattering of light in liquids and dense gases and the critical magnetic scattering of neutrons. This analogy forms the basis of Van Hove's theory[14] of magnetic scattering in this region.

Van Hove postulated an instantaneous spin-correlation function of the same type as that assumed in the classical Orstein-Zernike[27] theory of critical opalescence. This function has the form

$$\langle S_0^{\alpha}(0) S_R^{\alpha}(0) \rangle = \frac{V_0 S(S+1)}{12\pi r_1^2} \frac{e^{-\kappa_1 R}}{R}, \tag{9}$$

where V_0 is the volume of the crystal cell and κ_1 and r_1 represent, respectively, the range and strength of the spin correlations. The parameters κ_1 and r_1 are related to the static susceptibility by the expression

$$(\kappa_1 r_1)^2 = \chi_1 / \chi^{\alpha}(0), \tag{10}$$

where $\chi_1 = Ng^2\mu^2 S(S+1)/3kT$, i.e., the susceptibility of a system of noninteracting spins. For a formal description of paramagnetic spin fluctuations in iron, it is not necessary to retain the superscript α. It has, however, been suggested that this same form of correlation might apply below T_c (and also above T_c for anisotropic Hamiltonians in noncubic crystals) where the superscript α is necessary. We have therefore retained it for generality.

To include the time dependence of the spin correlations, Van Hove assumed that the equation governing the density of magnetization is of the diffusion type. It then follows that a plane wave of magnetization will decay as

$$\langle S^{\alpha}(\mathbf{q},0) S^{\alpha}(\mathbf{q},t) \rangle = \langle S^{\alpha}(\mathbf{q},0) S^{\alpha}(\mathbf{q},0) \rangle e^{-\Lambda q^2 t}, \tag{11}$$

where Λ is the diffusion constant and $S^{\alpha}(\mathbf{q},t)$ the spatial Fourier transform of $S_R^{\alpha}(t)$.

Once the spatial and temporal dependence of the spin-correlation function are specified, the form of the cross section can be obtained from Eqs. (4), (9), and (11). For a single crystal it is

$$\mathcal{S}(\mathbf{Q},\omega) = \frac{2}{3\pi} \frac{S(S+1)}{r_1^2} \frac{1}{\kappa_1^2 + q^2} \frac{\Lambda q^2}{\Lambda^2 q^4 + \omega^2}. \tag{12}$$

The available evidence indicates that (12) gives a remarkably good description of the angular and energy distribution of the scattered neutrons over a fairly wide range of q. This range, in effect, will define the hydrodynamic region. Equation (10), which relates the neutron scattering parameters to the static susceptibility, has also been demonstrated to be substantially correct. Indeed, critical neutron scattering has proved to be an excellent method of measuring the temperature dependence of the zero-field susceptibility in the neighborhood of the ordering temperature.

There is, however, a curious problem associated with the diffusion constant Λ. Van Hove, in his original formulation, assumed that the Onsager kinetic coefficient remains finite at the ordering temperature. This leads to the conclusion that Λ should vary as χ^{-1}. The scattering is therefore expected to become increasingly elastic near T_c as fluctuations in the magnetization decay more and more slowly. Iron is the only ferromagnet which has been studied in any detail and surprisingly the existing measurements (which may not have been entirely in the hydrodynamic region) show no evidence of the expected slowing down of the fluctuations.

This unexpected situation has stimulated a reexamination of the theory of spin diffusion in ferromagnetic systems and, recently, Kawasaki[28] has shown that Van Hove's original assumptions are not valid for a Heisenberg ferromagnet. Using a self-consistent formulation he found that Λ should vary approximately as $\chi^{-1/4}$ rather than χ^{-1}. Halpern and Hohenberg[18] came to the same conclusion using scaling-law arguments. Krueger and Huber[29] have further suggested that at temperatures more than a fraction of a percent above T_c there should be a downward departure from this power law.

Of course outside the hydrodynamic region the form of the spin-correlation function is expected to change considerably as the influence of propagating modes becomes more pronounced. But even within the hydrodynamic region, Fisher[30] has pointed out that small departures from (9) are to be expected. This is a consequence of the limitations of the Ornstein-Zernike theory itself and should occur in all types of critical scattering. The differences between (12) and the distributions predicted by Fisher are, however, very small and should only be significant at the smallest values of q.

III. EXPERIMENTAL TECHNIQUE

Most previous investigations of critical scattering from ferromagnets have been performed by observation of the scattering in the vicinity of the forward direction, corresponding to the use of the reciprocal-lattice vector $\tau = 0$. However, such techniques suffer from the fundamental restriction that at a given wave vector q the

[27] L. S. Ornstein and F. Zernike, Proc. Acad. Sci. Amsterdam **17**, 793 (1914).

[28] K. Kawasaki, J. Phys. Chem. Solids **28**, 1277 (1967).

[29] D. A. Krueger and D. L. Huber (private communication).

[30] M. E. Fisher, Physica **28**, 172 (1962).

maximum energy transfer that can be realized by neutron scattering is $2E_0q/k_0$. This has the adverse effect that parts of the frequency spectrum of the scattering cannot be observed. We have avoided this problem by taking all measurements near to a (1,1,0) reciprocal-lattice point with a triple-axis spectrometer.

A. Instrumental Resolution

To best interpret the experimental data it is necessary to study the resolution function of the spectrometer. The approach taken by Cooper and Nathans[31] is the one we have followed and will therefore be briefly described.

Suppose we wish to observe the neutron scattering function $S(\mathbf{Q},\omega)$ at some particular values of $\mathbf{Q}$ and ω, say $\mathbf{Q}'$ and ω'. The sensitivity of the spectrometer to particular values of $\mathbf{Q}$ and ω is defined by the function $R(\mathbf{A}',\Delta\mathbf{A})$, where $\mathbf{A}$ is a four-dimensional vector with components

$$A_1=Q_x,\quad A_2=Q_y,\quad A_3=2m\omega/\hbar,\quad A_4=Q_z. \quad (13)$$

The axes x, y, and z are chosen such that x is along $\mathbf{Q}'$ and z is in the vertical direction normal to $\mathbf{k}_0$ and $\mathbf{k}_1$. We have set $\Delta\mathbf{A}=\mathbf{A}-\mathbf{A}'$. Cooper and Nathans show that, subject to a number of reasonable assumptions, R is given by

$$R(\mathbf{A}',\Delta\mathbf{A})=C(\mathbf{A}')\exp(-\tfrac{1}{2}\Delta\mathbf{A}\cdot\mathbf{M}\cdot\Delta\mathbf{A}), \quad (14)$$

where $\mathbf{M}$ is a 4×4 matrix whose elements are calculable from the instrumental parameters. Contours of equal sensitivity of the instrument are ellipses in the four-dimensional space of $\mathbf{A}$ with the contour spacings following a Gaussian distribution.

We have confined our attention to the use of the instrument in the W configuration shown in Fig. 2. For scattering close to elastic with a symmetric collimation system (i.e., in the notation of Cooper and Nathans $\alpha_0=\alpha_3$, $\alpha_1=\alpha_2$, $\eta_M=\eta_A$), the ellipse of Eq. (14) has the following properties, assuming parameters of the sort normally used experimentally:

(1) Two axes of the ellipse are typically an order of magnitude larger than the other two.

(2) One of the two larger axes of the ellipse is along the z axis.

(3) The larger one of the two shorter axes is along the x axis.

(4) The other axes of the ellipse are in the y-ω plane with the larger one of them at between 5° and 20° to the energy axis.

Property (3), i.e., a short axis of the ellipse along the x axis, is particularly valuable for experiments requiring data to be taken at small values of q. This is due to the fact that at $q=0$ there is usually a Bragg peak present and also as q becomes very small many cross sections (magnon, phonon, critical scattering) tend to become very large and the scattering close to elastic. Thus it is essential that the ellipse not have any intensity at $q=0$. By restricting the experiment to wave vectors $\bar{q}$ along the x axis this condition can be satisfied for much smaller values of $\bar{q}$ that would otherwise be possible.

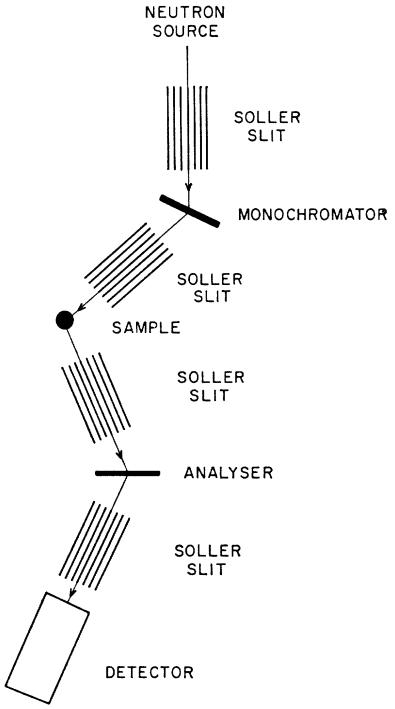

FIG. 2. Layout of the triple-axis neutron spectrometer used in the current experiment. The use of the instrument in the symmetric W formation can lead to high resolution along the direction of the scattering vector $\mathbf{Q}$ due to certain instrumental focusing properties.

The use of this experimental technique has enabled us to take meaningful data at wave vectors down to 0.02 Å^{-1}. The experimental conditions used for different parts of the experiment and their resolution functions at $\bar{Q}=3.1$ Å^{-1} and $\hbar\bar{\omega}=0$ are tabulated in Table I in roughly descending degree of resolution. The work near the critical temperature was all done with one of the four best resolution functions; usually with the second and third best sets of conditions. Broader resolution functions with incident energies of 65 and 100 meV were used when observing room-temperature magnons at large q vectors where the cross section is small and the energy transfer is high. These are not included in Table I since they were used only at energy transfers so large compared to the incident neutron energy as to radically affect the properties 1–4 of the ellipse listed above; thus, direct comparison of these resolution functions with those for near-elastic scattering cannot be made on any simple basis.

The strongly aspherical nature of the resolution function has a marked influence on experimental line

[31] M. J. Cooper and R. Nathans, Acta Cryst. 23, 357 (1967).

TABLE I. Some resolutions functions used for studying the magnetic scattering from iron with low energies. The focusing properties of the instrument have been exploited to give a very small spread in $\mathbf{q}$ values along the direction q_x while allowing much larger spreads along q_y and q_z.

E_0 (MeV)	Monochromator reflection	Mosaic (min)	Soller slit angles (min)	Resolution function ($Å^{-1}$) q_x	q_y-ω plane	q_z
9	Ge 111	3	10-40-40-10	0.0025	0.001; 0.029	0.047
9	Ge 111	15	20-10-10-20	0.0043	0.002; 0.029	0.047
9	Ge 111	15	10-40-40-10	0.0028	0.001; 0.043	0.047
13	Ge 220	15	20-30-40-20	0.0041	0.003; 0.050	0.056
13	Ge 111	15	20-20-20-20	0.0055	0.003; 0.071	0.056
20	Ge 220	15	20-30-40-20	0.006	0.003; 0.10	0.070

shapes. Previous investigations of line shapes[31,32] have concentrated on problems where there is a sharp magnon or phonon excitation. A Taylor expansion of the dispersion curve around $\mathbf{Q}'$ then yields a closed Gaussian form for the line shape. This treatment is not appropriate, however, for long-wavelength magnons such as the ones studied in the present experiment both because the curvature of the dispersion curve is appreciable over the extent of the resolution function and because the cross section itself itself varies significantly over this region. To predict experimental line shapes we have instead resorted to numerical integrations of the cross section over the resolution function.

Thus, if the cross section is expressed in terms of $\mathcal{S}(\mathbf{Q},\omega)$ or $\mathcal{S}(A)$, as defined by Eq. (1), the scattering intensity $I(\mathbf{A}')$ at the instrumental setting $\mathbf{A}'$ is given by the integral

$$I(\mathbf{A}')=\int \mathcal{S}(\mathbf{A})R(\mathbf{A}',\mathbf{A}-\mathbf{A}')d\mathbf{A}.$$

In order to evaluate the four-dimensional integral, we have rotated the coordinate system of $\mathbf{A}$ to that of the four eigenvectors of the matrix $\mathbf{M}$. This implies that the axes are then those of the resolution function ellipse defined by Eq. (14). Now the limits of the numerical integration can be placed at some appropriate low contour of this ellipse to make the integration just over values of $\mathbf{A}$ that contribute significantly to the scattering. We used the contour corresponding to three Gaussian widths from the center of the ellipse as the cutoff contour. For a few cases it was verified that the exact position of this cutoff did not appreciably affect the integral.

Experience indicated that for critical scattering or for scattering from broad magnons the integral could usually be evaluated to about 1% for a mesh of roughly 10 000 points. For sharp magnons, the cross section contains a δ function in its analytic form and it was necessary to do the integral over one dimension of $\mathbf{A}$ by hand to eliminate that δ function. For the remaining three-dimensional integral it was found that typically a mesh of 20 000 points gave an accuracy of about 1%. The results of such a set of integrations are compared to experiment in Fig. 3. The strong asymmetry in the magnon peaks is clearly evident; there is a very satisfactory fit to the experimental data except for a single case ($T=300°K$, $q=0.03$ $Å^{-1}$) which we do not understand. The arrow shows where the peak would occur if an instrument with very high resolution were used. The magnon energy cannot be accurately identified with the peak in the experimental scattering cross section; the area center of the cross section gives an even less reliable value of the magnon energy. It is clear that considerable care is needed to interpret data of this kind. Near T_c, however, the dispersion curve has less curvature and the distortion of the magnon peaks becomes less pronounced.

The sharp cutoff in the scattering at the low-energy side is a consequence of the use of the instrument in the way described above. It is a most useful experimental technique since it facilitates accurate determination of magnon energies and linewidths.

Just below the Curie temperature where intrinsically broadened magnon peaks are observed we always identified the peak in the scattering cross section as the magnon energy. The relaxation can in itself produce a shift of the peak, but since the magnitude of that shift depends on the mechanism for the broadening we have not tried to correct for this effect. The point should perhaps be made that theories of magnon energy renormalization near T_c should state explicitly how the magnon energy is to be defined for such broadened excitations.

In the hydrodynamic region, detailed least-squares fits were made to compare the scattering with the diffusive form of the cross section given by Eq. (12). For such fits to be meaningful, it is necessary to know the parameters of the resolution ellipse with some confidence. The Bragg peak provides a convenient way of comparing the calculated parameters with observations, although the measurements are necessarily confined to the point $\mathbf{Q}=\boldsymbol{\tau}$ and $\omega=0$. For the instrumental parameters used in the present experiment, we have found that the axes of the ellipse are within 2° of their predicted directions, while the lengths of these axes, as determined from the half-height contour, are always within 10% of the calculated values. In the wings the contours are found to decay more steeply

[32] M. F. Collins, Brit. J. Appl. Phys. 14, 805 (1963).

than the Gaussian form of Eq. (14); this is believed to be due to the triangular form for the actual transmission of Soller slits rather than the Gaussian form assumed in the theory.

B. Sample

The iron specimen was in the form of a cylinder $\frac{1}{2}$ in. in diameter and 1.5 in. long. The [1$\bar{1}$0] crystal axis was along the cylinder axis and was mounted vertically. All measurements were taken near the (110) crystal reflection. The mosaic spread of the crystal was less than 5 min full width at half-height.

The iron crystal was mounted coaxially inside a hollow copper cylinder 2 in. in diameter, 5 in. in length, and 0.125 in. thick. The cylinder wall was thinned to 0.04 in. where the neutron beam passed through it.

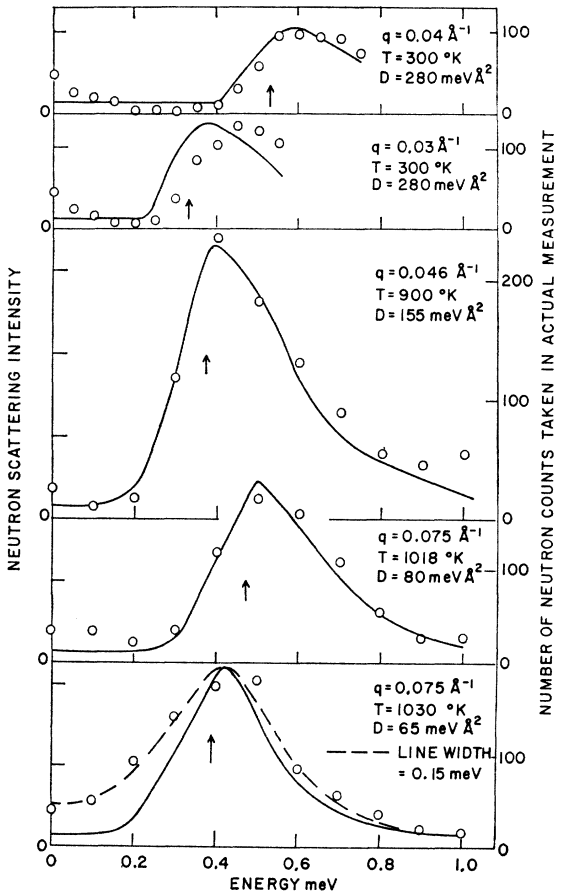

FIG. 3. Typical high-resolution magnon peaks in the scattering at different temperatures. The marked asymmetry of the peaks arises from aspherical nature of the instrumental resolution function and the curvature of the magnon dispersion curves. The arrows show the magnon energy calculated to be observed in the absence of instrumental resolution corrections. The solid lines represent the calculated peak shapes for magnons with exchange stiffness constants D as marked and with a dipole-dipole term included. The dashed line on the highest-temperature data is the calculated peak shape for a magnon with an intrinsic linewidth of 0.15 meV.

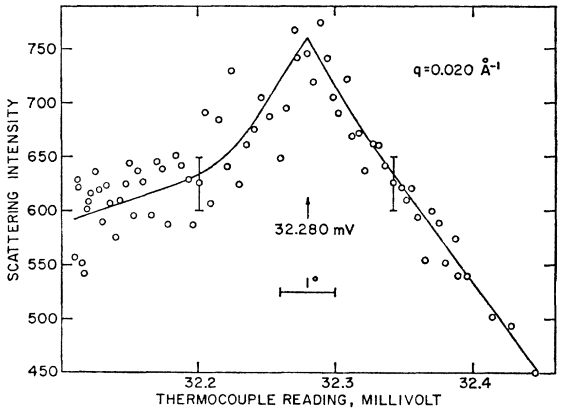

FIG. 4. High-resolution study of the temperature dependence of the scattering at $q=0.02$ Å^{-1} and $\omega=0$. The location of the peak in the scattering serves to define the critical temperature.

Irises on the incident and scattered neutron beams of a size just larger than that of the specimen ensured that no single scattering event from the copper was transmitted by the instrument.

Outside the copper cylinder a cylindrical heater mesh of molybdenum was mounted, followed by three radiation shields and the furnace wall. The furnace was maintained under vacuum. The copper cylinder served to give a temperature uniformity over the specimen of better than 0.5°. A proportional temperature-control system kept the sample temperature constant over long periods to within about 0.5° to 1°.

C. Determination of T_c

T_c was measured by observing the scattering cross section as a function of temperature with the instrument set for $\bar{\omega}=0$ and $\bar{q}=0.02$ Å^{-1} or 0.025 Å^{-1} and other instrumental parameters set for high resolution (cf. Table I). A typical set of data is shown in Fig. 4. There is a sharp peak in the scattering which is defined to within about 0.1°. The transition temperature T_c is derived from the location of this peak. Similar measurements at larger values of $\bar{q}$ gave peaks which were much broader and were shifted somewhat to higher temperatures.

The measurement of T_c was checked periodically throughout the experiment; no appreciable drifts in its value were detected.

IV. EXPERIMENTAL RESULTS

A. Spin-Wave Region

Extensive measurements of the spin-wave dispersion relation were made at room temperature. The data extend to both lower and higher wave vectors than those used in the other neutron experiments employing scattering surface techniques.[1,2]

Figure 5 shows the spin-wave energy plotted against wave vector q. Near the zone boundary the spin-wave

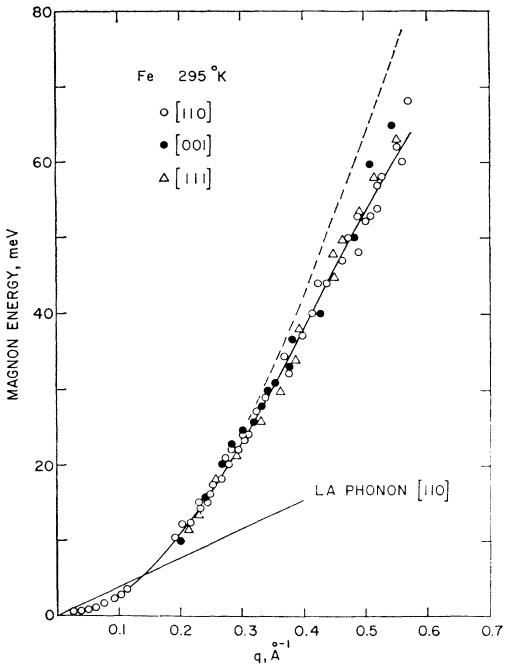

FIG. 5. The spin-wave dispersion relations in iron at room temperature. The dashed curve shows the predicted dispersion relation for a nearest-neighbor Heisenberg Hamiltonian along the 110 direction. The solid line shows the values for the dispersion relation $E=281q^2-275q^4$ meV. The magnon energy appears to be virtually independent of its direction of propagation and can only be described in terms of the Heisenberg Hamiltonian if long-range exchange forces are invoked.

energy becomes rather high for neutron scattering techniques and in fact our data only extend about 40% of the way to the zone boundary. All the small q data was taken along the 110 crystal direction near the 110 Bragg peak both to utilize the focusing properties of the ellipse as discussed in Sec. III A and to

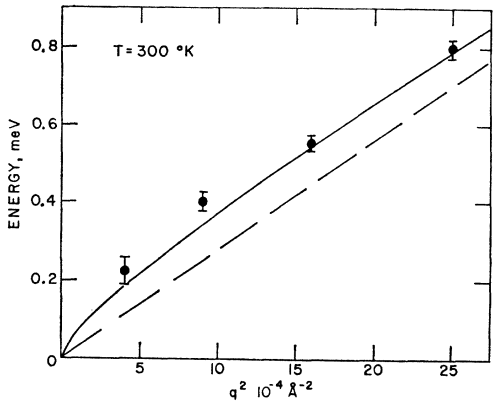

FIG. 6. Spin-wave energies plotted against q^2 in iron at room temperature. The data were taken at high resolution from small wave vectors in the range $0.02<q<0.05$ Å^{-1}. The Heisenberg Hamiltonian alone (dashed line) will not describe these data, though the inclusion of a dipole-dipole term in the Hamiltonian (solid line) does give a satisfactory description.

retain an appreciable value for the form factor $f(\mathbf{Q})$ in the scattering cross section. For q values larger than 0.2 Å^{-1} data were taken along all the three principal high-symmetry directions of a cubic crystal, i.e., [100], [110], and [111]. As can be seen from Fig. 5, no appreciable directional anisotropy of the spin-wave energies was detected. The data for these larger q values were all taken with constant-E plots rather than the constant-$\mathbf{q}$ plots used at small q.

Figure 6 shows high-resolution measurements of the spin-wave energies plotted against q^2 for low wave vectors in the region $0.02<q$ 0.05 Å^{-1}. The data highlight the need for the inclusion of the dipole-dipole term in the Hamiltonian, which results in the magnon dispersion relation expressed by Eq. (6). There is a clear departure from the purely Heisenberg Hamiltonian of Eq. (5) (dotted line) but when the dipole-dipole term is added (solid line) there is satisfactory agreement between theory and experiment. In calculating the dipole-dipole term, the domains in the specimen were assumed to be randomly distributed among the six ⟨100⟩ easy directions of magnetization.

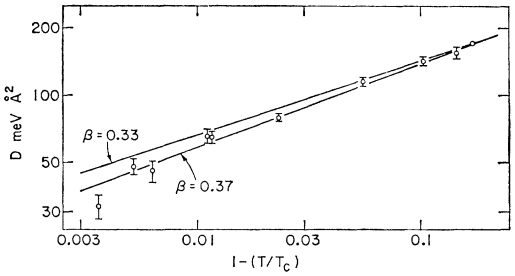

FIG. 7. The spin-wave constant D plotted against $1-T/T_c$ on a log-log scale. The linear fit shows that the spin-wave energies are being renormalized to zero at T_c following a power law which is very close to that followed by the magnetization.

This is the first direct demonstration with neutron scattering techniques of the necessity for including this term in the Hamiltonian, although the data of Stringfellow[2] indirectly point to its existence through anomalous line shapes in the small-angle neutron scattering pattern.

Our data can be fitted satisfactorily at all q values with a dispersion relation given by Eqs. (5) and (6) with

$$D=281\pm10 \text{ meV Å}^2$$

and

$$E=-270\pm35 \text{ meV Å}^4.$$

The intrinsic linewidth η is too small to be significant. The fit corresponds to the solid lines drawn in Figs. 5 and 6. It is of interest to compare this fit with the predicted dispersion relation for nearest-neighbor-only Heisenberg exchange. If the experimental value of D is used to determine the nearest-neighbor exchange constant, the model predicts that E should have values

of -48, -96, and -112 meV Å^4 for the [100], [110], and [111] directions, respectively. The 110 dispersion relation predicted by the model is shown by the dashed curve in Fig. 5. The experimental value of E is much greater than the model predicts and does not show the expected anisotropy. It is clear from the unsatisfactory fit to this simple model that exchange in iron must be of long range. This is one of the few properties of the magnetism of iron in which its metallic nature is clearly apparent.

At elevated temperatures we have continued to interpret our data in terms of the spin-wave dispersion relations given by Eqs. (5) and (6). The fit is satisfactory throughout the spin-wave region. The term in Dq^2 dominates the dipole-dipole term and the term in Eq. (4) for the range of wave vectors used. We will report only our experimental values for the parameter D. Near T_c the spin-wave modes have a linewidth comparable with their own energy and in this region we have identified the peak in the scattering cross section at constant $\mathbf{q}$ as the spin-wave energy.

Figure 7 shows the experimentally derived values of D plotted against $1-T/T_c$ on a log-log scale. The plot can be fitted with a straight line of slope 0.37 ± 0.03, showing that over the temperature range of the data ($0.005<1-T/T_c<0.2$), D varies as $1-T/T_c$ to the power 0.37 ± 0.03. Contrary to the data of Stringfellow[2] there is no evidence that D remains finite at T_c. We have observed spin waves at temperatures below T_c with energies almost a factor of 2 smaller than the value he obtains for the spin-wave energy at and just above the Curie temperature. It is probable that his use of a magnetic field of around 3000 Oe was responsible for the difference. According to Stringfellow, the field that he used was sufficient to induce a magnetization at the Curie temperature of 20% of the low-temperature value. Thus, it is not unlikely that the applied field had a profound effect on the spin-wave energy.

The variation of $\chi(q)$ with temperature can be determined by integrating the areas under the curves in Fig. 3. Just by inspection, it is evident that $\chi(q)$ varies roughly with the absolute temperature until T is near T_c, then $\chi(q)$ begins decreasing as T approaches T_c. Figure 8 shows the temperature variation of $\chi(q)$ within a narrow range near T_c. In this restricted interval, $\chi(q)$ is essentially independent of temperature below T_c. All of these data can be summarized by stating that $\chi(q)$ is roughly proportional to T/q^2 below T_c.

The standard low-temperature form of the cross section for a Heisenberg ferromagnet gives a susceptibility $\chi(q)$ which varies as T/Dq^2 so long as $kT\gg Dq^2$. The observed variation of $\chi(q)$ indicates that this is wrong by a factor of the order of D [i.e., $(T_c-T)^{0.37}$ near T_c]. Just such an effect has been recently predicted by Marshall and Murray,[33] who show that kinematic spin-wave interactions should produce an additional term in the cross section of the type $\langle S^z\rangle$. Near T_c this term is known to behave something like $(T_c-T)^{1/3}$ and so could account for the discrepancy.

Stringfellow[3] has already made a study of scattered intensities, particularly at temperatures below the critical region. We have not attempted to make a complete set of measurements in this temperature

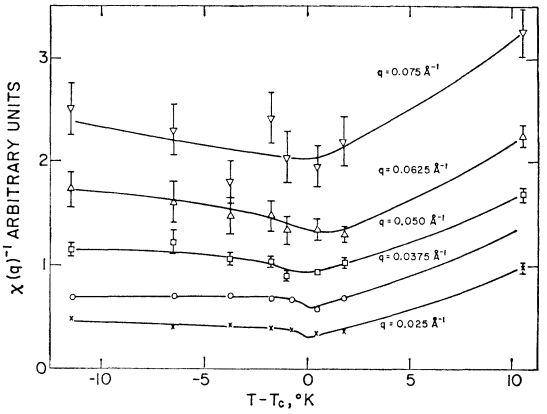

FIG. 8. The inverse static wavelength-dependent susceptibility plotted against temperature near T_c. The temperature dependence is only weak below T_c, but it is much more marked above T_c.

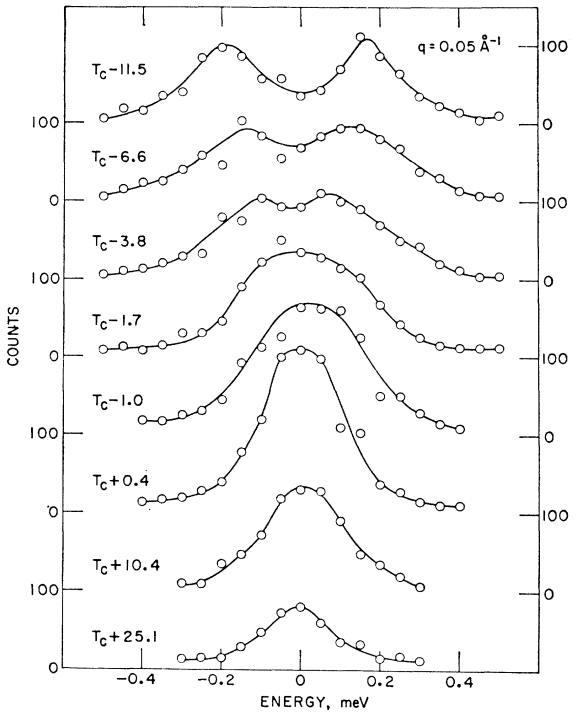

FIG. 9. The scattering at $q=0.05$ Å^{-1} plotted as a function of temperature. The well-defined magnons at $T_c-11.5°$ rapidly lose energy and become very broad until critical damping is apparent near $T_c-3°$. Linewidths decrease rapidly until the temperature reaches T_c, after which there is only a slow variation. The integrated intensity of the scattering only varies slowly with temperatures below T_c, but it falls off rapidly above T_c.

[33] W. Marshall and G. Murray, J. Appl. Phys. **39**, 380 (1968).

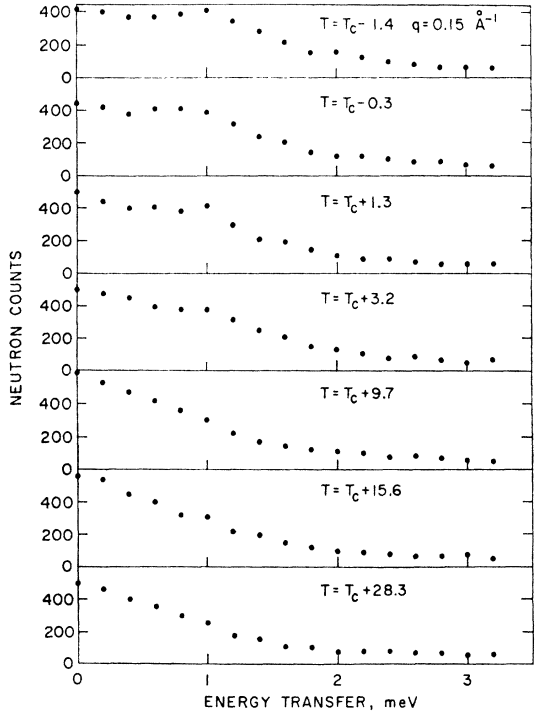

FIG. 10. The scattering at $q=0.15$ Å^{-1} plotted as a function of temperature. In contrast to the data at $q=0.05$ Å^{-1} of Fig. 9, there are no sharp changes in the scattering just below T_c. The scattering at the four lower temperatures is a very flat-topped function which can be imagined as having some sort of a shoulder at around 1 meV energy.

range. Nevertheless, our limited data confirms the existence of an additional term in the cross section with general properties similar to those proposed by Marshall and Murray.

The neutron scattering at a wave vector q of 0.05 Å^{-1} at various temperatures near to T_c is shown in Fig. 9. At $T_c-11.5°$, the lowest temperature in the figure, the spin-wave linewidth is already appreciable when compared to the instrumental resolution. This linewidth increases as the temperature is increased until the spin wave becomes over-critically damped at a temperature roughly 3° below T_c. This over-critical damping at a temperature below T_c has been observed for all the wave vectors studied in the present work (from 0.025 to 0.175 Å^{-1}). It precludes us from being able to say whether or not D actually goes to zero at T_c. Once the spin waves become over-critically damped, D ceases to be a useful parameter since it cannot be readily extracted from the experimental data. All that can be done is to point out that the data of Fig. 7 shows D follows a power law in T_c-T for nearly two decades of temperature. It therefore appears that the spin-wave energies are renormalized to zero at T_c for data taken within the spin-wave region.

There is no indication of a third peak in the cross section centered at zero energy in the data taken in the spin-wave region. The absence of a central peak is evident in both the high-temperature data of Fig. 3 and the low-temperature data of Fig. 9. Such a peak could arise from a diffusive component in χ^z near T_c with a spin-correlation function and a cross section as described by Eqs. (9) and (12). A central peak has been observed in the antiferromagnet $RbMnF_3$ by Nathans, Menzinger, and Pickart[34] at temperatures down to at least $0.9T_c$. If a similar peak exists

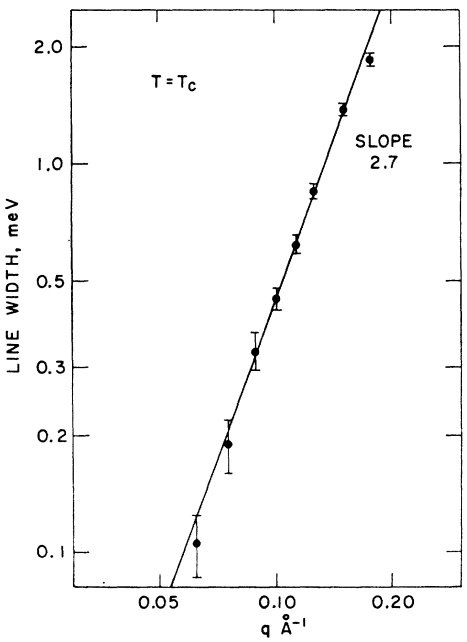

FIG. 11. Half-width at half-height of the scattering function at temperature T_c plotted against wave vector q on a log-log scale. The data have been corrected for instrumental contributions to the width. The line drawn through the points corresponds to a power law of 2.7. Halperin and Hohenberg have predicted a power law of 2.5.

in iron, either its cross section must be almost an order of magnitude smaller than the magnon cross section or its energy width must be very much larger. Also, there is no evidence of a propagating mode in χ^z, although it is possible, of course, that such a mode exists in an energy range outside that used for the scans made in collecting our data.

The absence of a contribution from χ^z to the scattering in the spin-wave region at temperatures near T_c is very puzzling. It makes it all but impossible to establish the boundary between the spin-wave and the transition regions. In fact it is not even clear if such a pair of regions with a boundary between them is a useful concept. The only boundary that we can see in the experimental data is the line of critical damping for the magnons. It is sufficient for our purposes to arbitrarily call this the boundary between the regions.

[34] R. Nathans, F. Menzinger, and S. J. Pickart, J. Appl. Phys. 39, 1237 (1968).

B. Transition Region

The lack of any theoretical framework gives a discussion of the data in the transition region a more qualitative nature then in the other two regions. However, since no experimental details of dynamical behavior in the transition region have been given before, even a qualitative discussion is of value in highlighting the features which must be included in any future theoretical discussion.

On entering the transition region from the spin-wave region, Fig. 9 for $q=0.05$ Å^{-1} shows that the linewidth of the peak centered about zero energy narrows rapidly until $T=T_c$. Above this temperature the linewidth does not change rapidly with temperature.

In contrast $\chi(\mathbf{q})$, as defined by Eq. (3), varies slowly with temperature for $T<T_c$ but then varies more rapidly for $T>T_c$. This can be clearly seen in Fig. 8 and is also evident in the integrated area of the data in Fig. 9.

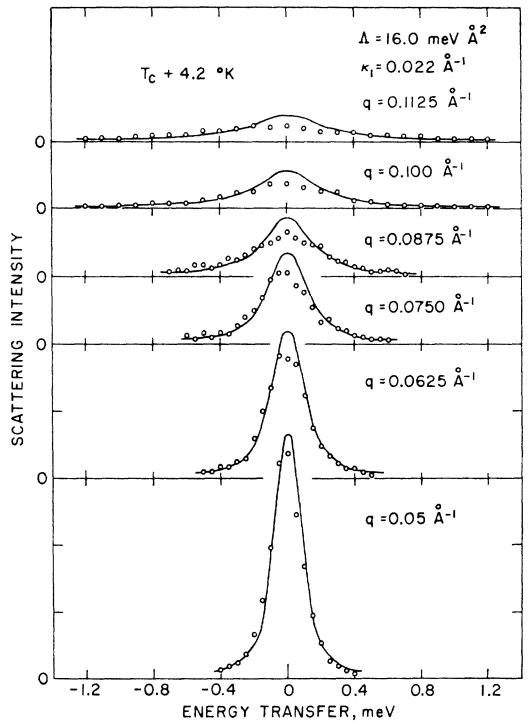

FIG. 12. The scattering at $T_c+4.2°$ plotted as a function of wave vector q. The size of the circles corresponds roughly to the energy resolution. The solid lines show the predicted scattering on the basis of the diffusion equations using parameters extrapolated from data at higher temperatures in the hydrodynamic region. The poor fit illustrates the breakdown of the diffusion equations on passing into the transition region.

Figure 10 shows the variation of the scattering across the transition region for the larger q value of 0.15 Å^{-1}. Here, in contrast to the data at 0.05 Å^{-1} of Fig. 9, there is no rapid narrowing of the line in the region of temperature between $T_c-1.5°$ and T_c. The linewidth steadily decreases throughout the transition region as the temperature is increased. It is a general feature of our data that at the smaller values of q the linewidths vary rapidly at temperatures just below T_c while at larger values this effect becomes progressively less pronounced and the data shows little change on passing through the critical temperature. The data of Fig. 10 for $q=0.15$ Å^{-1} shows moderately well-defined shoulders for the three or four lower temperatures; between $T_c-1.4°$ and $T_c+3°$. As the temperature is raised these shoulders gradually disappear and the peak shape changes into the Lorentzian form characteristic of the hydrodynamic region.

In view of the evidence of Fig. 7 that the spin-wave energies go to zero at T_c, it is difficult to know whether or not in fact these shoulders should be regarded as remnants of spin-wave excitations. The data certainly suggest that there is some sort of propagative component in the magnetic fluctuations. Possibly the spin-wave energy goes to zero at T_c only within the spin-wave region but within the transition region the energy is not renormalized to zero. However, the imaginary part of the spin-wave energy, which corresponds to the relaxation, is always of the order of or larger than the real part. Any theory of spin dynamics within the transition region would require a discussion of the behavior of both the real and the imaginary parts of the energy.

The widths at half-height of the lines at $T=T_c$ are shown in Fig. 11 on a log-log plot against the wave

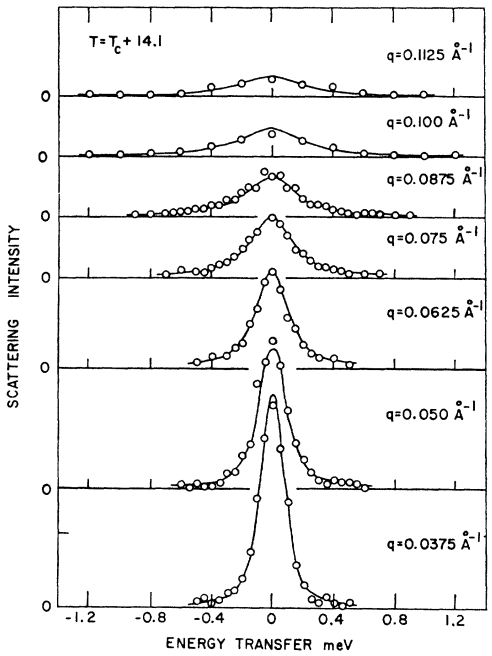

FIG. 13. The scattering at $T_c+14.1°$ plotted as a function of wave vector q. Up to tenfold larger counting times were employed for the larger q values. The solid line is the predicted scattering on the basis of the diffusion equations.

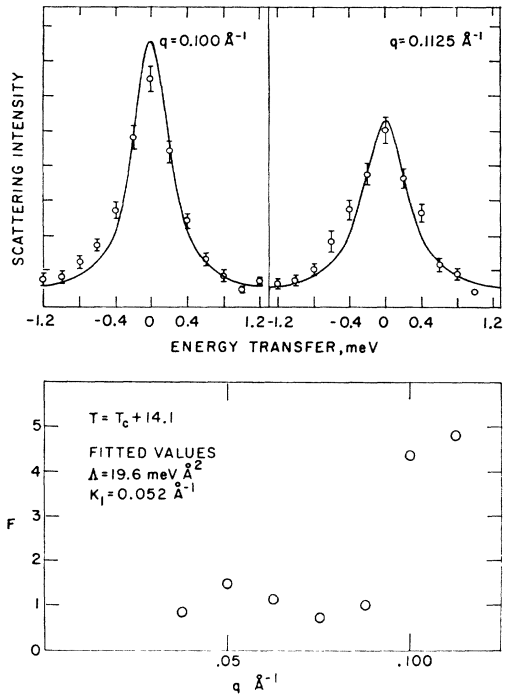

FIG. 14. The upper part shows the two largest q values of Fig. 13 plotted on an expanded scale with the statistical accuracy of the observed intensities indicated. The lower part shows the F factor for goodness of fit for the data of Fig. 13 after a least-squares fitting with disposable parameters κ_1, Λ, and r_1. The fit is good for $q \leq 0.0875$ Å^{-1} but significant departures occur at larger values of q.

vector q. The resolution function has been subtracted from these widths in an approximate manner. The uncertainties in the linewidths for the smaller wave vectors become relatively large because of the resolution correction and also because the widths themselves vary rapidly with temperature close to $T=T_c$ in this region. The plot of Fig. 11 is a straight line showing that the width varies as q to the power 2.7 ± 0.3. This is within the error, the same as the value 2.5 predicted by Halperin and Hohenberg.[18] Our experimental data have thus confirmed two predictions of the dynamic scaling laws, viz., the q dependence of the linewidth at T_c and the temperature dependence of the spin-wave stiffness constant D. Both these predictions were made in advance of the existence of experimental data; they constitute a notable success for the theory.

In Fig. 12 the line shapes are shown for a range of wave vectors at a temperature of $T_c+4.2°$. The solid lines show the predicted line shapes. They are calculated from Eq. (12) with parameters appropriate to the hydrodynamic region at the temperature at which the data was taken. Peaks in the transition region are broader and more square-shaped than in the hydrodynamic region. $\chi(q)$, as reflected by the integrated areas of the curves in Fig. 12, varies more slowly than the linewidths on moving from the hydrodynamic to the transition region, though in general $\chi(q)$ is smaller than would be predicted on the basis of the Lorentzian form.

It is evident in Fig. 12 that only extremely high resolution will suffice to remain within the hydrodynamic region at a temperature 4.2° above T_c. Considering the resolution available, previous measurements of critical scattering from iron at temperatures less than $T_c+10°$ were almost surely made in the transition region.

C. Hydrodynamic Region

Above T_c we expect to find a region defined as the hydrodynamic region in which diffusion theory applies. We have shown in Fig. 13 the distributions observed at $T_c+14.1$°C. On this same figure, we have also plotted the best-fitting curves obtained by folding the diffusion-model cross section [Eq. (12)] with the spectrometer resolution function. The details are described in the Appendix. Clearly, there is good agreement over an extended range of q. The scattering is well represented by the two disposable parameters κ_1 and Λ.

The results of the fitting appear in the lower part of Fig. 14. It can be seen that at $T_c+14.1$°C, for $q \leq 0.0875$ Å^{-1}, the fitting parameter "F" defined in the Appendix is near unity, indicating an acceptable fit. At the largest values of q, however, F increases abruptly, indicating that the data are not adequately represented by the calculated curves. We have interpreted this as implying that we have reached the boundary of the hydrodynamic region. A similar, rather well-defined boundary, appears in all our data at q values of $1.5\kappa_1$ to $2.0\kappa_1$.

To see in detail how the experimental distributions outside the hydrodynamic region differ from the Van Hove form [Eq. (12)], we have replotted the two largest values of q in Fig. 13 on an expanded scale in the upper part of Fig. 14. The observed distributions show a small but significant broadening which becomes more pronounced as the measurements extend further into the transition region (cf. Fig. 12). This broadening cannot be explained solely in terms of a q^4 term in the cross section.

According to the discussion in Sec. II B 3, the parameters of primary theoretical interest are Λ and the product $\kappa_1 r_1$. The latter is related to the static susceptibility $\chi(0)$ through Eq. (10). Once the Van Hove parameters are fitted to the data, $\chi(0)$ is easily determined since κ_1 is known and the normalization constant $\mathfrak{N}$ is proportional to r_1^{-2}. Thus, $\mathfrak{N}/\kappa_1^2$ is proportional to $\chi(0)$.

We have plotted $\mathfrak{N}/\kappa_1^2$ against $(T-T_c)/T$ on a log-log scale in Fig. 15 using data extending over a temperature range from T_c+8°C to T_c+51°C. From the slope of the best-fitting straight line through the points, we find that $\chi(0)$ varies as $[(T-T_c)/T]^{-\gamma}$, where $\gamma=1.30\pm0.06$. This value is in excellent agree-

ment with values obtained both by previous measurements of critical neutron scattering[3–6] and by measurements of the static susceptibility.[35–37] A consensus of all the experimental data (including this work) indicates that γ must lie between 1.30 and 1.34; however, recent theory suggests it to be between 1.38 (Refs. 38 and 39) for $S=\infty$ and 1.43 for $S=\frac{1}{2}$.[40]

We are not able to obtain reliable values for the Van Hove parameters at temperatures less than $T_c+8°C$ because the range of the hydrodynamic region becomes so restricted. The resolution requirements at these temperatures are extreme and, in fact, it is reasonable to suppose that the lowest temperature value of $(\kappa_1 r_1)^2$ in Fig. 15 lies below the line because the distributions, even at this temperature, become sensitive to the smallest errors in the resolution analysis.

While it is gratifying to note that there is good agreement among the various groups on the value of the exponent γ, the agreement on the values of κ_1 is less satisfactory. The reasons for this are not hard to find. From Eqs. (3) and (12) it is easy to show that the static susceptibility $\chi(q)$ is of the form

$$\chi(q)=\frac{g^2\mu^2 S(S+1)}{3kT}\frac{1}{r_1^2(\kappa_1^2+q^2)}.$$

It is evident that the product $(\kappa_1 r_1)^2$ is determined in effect by extrapolating from the scattering observed at finite values of q to the value at $q=0$. But to obtain κ_1 alone, it is necessary to extrapolate considerably further in order to find the value of q for which $1/\chi(q)=0$. Thus, a larger error in κ_1 is to be expected. Fortunately, the principle interest has not been in κ_1 but in $(\kappa_1 r_1)^2$, which can be more accurately determined.

Let us turn now to the parameter Λ, which is related to the dynamics of the spin fluctuations. Using only data within the hydrodynamic region, we obtained the values for Λ shown in Fig. 15. The temperature variation of Λ evident in the figure can be described in terms of a simple power law with exponent 0.14 ± 0.04. No doubt there are other analytic forms which would fit equally well. In any event the important fact is that the exponent has about 40% of the expected value. Unfortunately, we were not able to obtain any data bearing on the crucial question of the behavior of Λ near T_c because the hydrodynamic region is simply too restricted.

This restriction explains certain puzzling features of the earlier measurements.[3–6] Thus, the deviation from a simple power law, which appears in Fig. 11 of Ref. 4, is no doubt a consequence of the fact that the data below $T_c+10°C$ was taken in the transition region. Also, it is not surprising that in the same experiment there was no difference in the values of Λ observed at $T_c+2°C$ and at $T_c+18°C$. At $T_c+2°C$ the measurements of Ref. 4 were made in the transition region where the distribution is broadened. The measurement of Λ at $T_c+18°C$ was, however, within the hydrodynamic region and is in reasonable agreement with ours as would be expected.

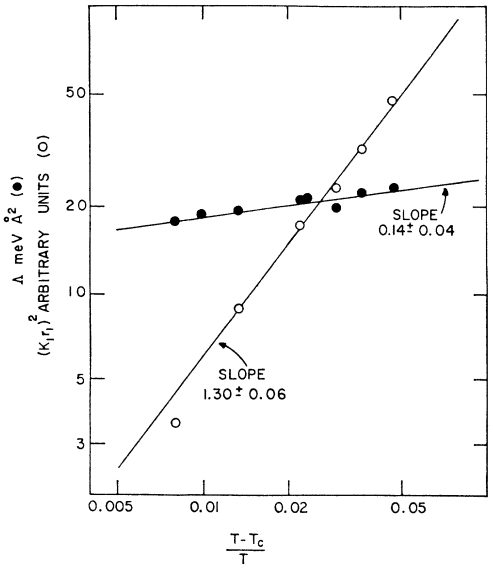

FIG. 15. $(\kappa_1 r_1)^2$, which is directly proportional to the static susceptibility, and Λ, the diffusion constant, plotted against $1-T_c/T$ on a log-log scale. Power laws with exponents 1.30 ± 0.06 and 0.14 ± 0.04, respectively, are obtained. (To obtain the value of the dimensionless parameter $2m\Lambda/\hbar$, multiply the corresponding value of Λ by 0.483.)

Because the hydrodynamic region is so restricted it is doubtful whether it is within the scope of current neutron scattering techniques to determine the exact form of the spin-correlation function in a ferromagnet, particularly with regard to an investigation of the Fisher parameter η[28]. Certainly no existing experimental data, including ours, are of sufficient quality to throw light on this matter.

V. CONCLUSIONS

Although Sec. IV contains detailed interpretations of the experimental data, it is valuable to summarize the results of our measurements.

First, the data establish four numerical laws; three of these have not been previously determined.

(1) Spin-wave energies appear to be renormalized to zero at the Curie temperature. The stiffness constant D varies as T_c-T to the power 0.37 ± 0.03, which is close to the power 0.33 predicted by Halperin and Hohenberg.

[35] S. Arajs and R. V. Colvin, J. Appl. Phys. Suppl. **35**, 2424 (1964).
[36] J. E. Noakes, N. E. Tornberg, and A. Arrott, J. Appl. Phys. **37**, 1264 (1965).
[37] G. Develey, Compt. Rend. **260**, 4951 (1965).
[38] C. Domb and M. F. Sykes, Phys. Rev. **128**, 168 (1962): J. L. Gammel, W. Marshall, and L. Morgan, Proc. Roy. Soc. (London) **A275**, 257 (1963).
[39] H. E. Stanley, Phys. Rev. **158**, 546 (1967).
[40] G. A. Baker, H. E. Gilbert, J. Eve, and G. S. Rushbrooke, Phys. Rev. **164**, 800 (1967).

(2) At the critical temperature the linewidth varies as the wave vector q to the power 2.7 ± 0.3, in satisfactory agreement with the value of 2.5 predicted by Halperin and Hohenberg.

(3) The spin-diffusion constant Λ varies as $1-T_c/T$ to the power 0.14 ± 0.04. This is a much slower variation than the power 0.33 predicted by Kawasaki and by Halperin and Hohenberg.

(4) The inverse static susceptibility varies as $1-T_c/T$ to the power 1.30 ± 0.06. A consensus of all the experimental data on this relation indicates a power law with exponent between 1.30 and 1.34 while the theory indicates an exponent of 1.38 for $S=\infty$ and 1.43 for $S=\frac{1}{2}$.

Second, a number of more qualitative conclusions can be drawn from the data.

(5) In the spin-wave region no peak has been detected in the scattering centered about zero-energy transfer; such a peak would correspond to diffusive motions of the spins.

(6) The line shape of the scattering in the transition region indicates a propagating component in the susceptibility even at temperatures above the critical temperature.

(7) Below T_c, $\chi(q)$ varies very slowly with T_c-T; this is taken to indicate that the spin-wave cross section varies in the general manner proposed by Marshall and Murray, even at temperatures close enough to T_c so that their low-temperature expansion might not be expected to remain valid.

(8) $\omega^{-1}\chi(q,0)$ has a very sharp peak at $T=T_c$ for the smaller wave vectors used. At larger values of q this peak shifts to a higher temperature and becomes less well defined.

(9) Data taken at larger wave vectors q seem to vary continuously through the critical temperature without any indication of the exact location of that temperature.

(10) All earlier experimental data on critical scattering from iron was not in the hydrodynamic region at temperatures below about $T_c+10°$. The interpretation of such data below this temperature is an involved and indirect process; in particular it is not practical to use it to investigate the magnitude of Fisher's parameter η. There are extreme difficulties in attempting to use neutron scattering techniques to investigate the hydrodynamic region when T is less than about $T_c+5°$.

(11) Comparison of our data with that of Stringfellow indicates that an applied magnetic field of 3000 Oe radically alters the long-wavelength spin dynamics near the critical temperature.

(12) The low-temperature spin-wave spectrum clearly exhibits the influence of the dipole-dipole term in the Hamiltonian.

(13) The low-temperature spin-wave spectrum indicates that exchange terms of the Heisenberg type must be of long range in iron.

Finally, we point out some outstanding unsolved problems which the present work has raised.

(14) Why does Λ vary so slowly with $T-T_c$? Does it go to zero at T_c?

(15) What is the nature of the propagative component of the spin dynamics in the transition region?

(16) Why has no diffusive peak been observed in the scattering below the critical temperature?

(17) If we could go out to large enough wave vectors q, would we see magnons less than critically damped above T_c?

(18) To what extent are the critical properties the reflection of a true Heisenberg ferromagnet and to what extent are they reflections of the metallic nature of iron?

ACKNOWLEDGMENTS

We are grateful to Dr. J. Skalyo, Jr., for his assistance during the course of this work. It is also a pleasure to acknowledge our obligation to Dr. M. Blume, Dr. P. Martin, and Dr. P. Hohenberg for helpful discussions of the theory.

APPENDIX

The following procedure was used to fit the cross section given by Eq. (12) to the experimental data. There are three disposable parameters κ, Λ, and $\mathfrak{N}$, where $\mathfrak{N}$ is an intensity normalization constant.

Preliminary values of κ_1 and Λ were estimated from the measurements of Ref. 4. Using these values, the resolution-corrected cross section was first normalized in intensity to the observed distributions by the method of weighted least squares. Then, to assess the adequacy of fit, the quantity

$$F=\frac{1}{N-m}\sum_{n=1}^{N}\frac{[I_n(\text{obs})-I_n(\text{calc})]^2}{I_n(\text{obs})}$$

was calculated for the N data points which determined the normalization. $I_n(\text{obs})$ and $I_n(\text{calc})$ represent, respectively, the individual observed and calculated intensities and m is the number of fitted parameters (three in this case). Thus, for each pair of values of κ_1 and Λ, we obtained a corresponding value of F.

After establishing the value of F for the initial choice of κ_1 and Λ, the values of these parameters which minimized F were determined by iteration. Concurrently, the range of q was varied to determine the limits of the region over which the choice for best fit was independent of q.